

RADIO FOLLOW-UP OF A CANDIDATE γ -RAY TRANSIENT IN THE SKY LOCALIZATION AREA OF GW170608

KYLE ARTKOP¹, RACHEL SMITH¹, ALESSANDRA CORSI¹, SIMONA GIACINTUCCI², WENDY M. PETERS², ROSALBA PERNA^{3,4},
S. BRADLEY CENKO^{5,6}, TRACY E. CLARKE²

Draft version March 6, 2021

ABSTRACT

After the identification of a candidate γ -ray transient in the error region of the binary black hole (BBH) merger GW150914 by the *Fermi* satellite, the question of whether BBH mergers can be associated to electromagnetic counterparts remains highly debated. Here, we present radio follow-up observations of GW170608, a BBH merger that occurred during the second observing run (O2) of the Advanced Laser Interferometer Gravitational-wave Observatory (LIGO). Our radio follow up focused on a specific field contained in the GW170608 sky localization area, where a candidate high-energy transient was detected by the *Fermi* Large Area Telescope (LAT). We make use of data collected at 1.4 GHz with the Karl G. Jansky Very Large Array (VLA), as well as with the VLA Low-band Ionosphere and Transient Experiment (VLITE). Our analysis is sensitive to potential radio afterglows with luminosity densities $L_{1.4\text{GHz}} \gtrsim 6 \times 10^{28} \text{ erg s}^{-1} \text{ Hz}^{-1}$. In the most optimistic theoretical models, $\approx 20\%$ of BBH events occurring in massive hosts could be associated with outflows as radio luminous as this. Although we find no evidence for the presence of a radio counterpart associated with the LAT candidate in the GW170608 error region, our analysis demonstrates the feasibility of future radio follow-up observations of well localized BBHs. Comparing our radio upper-limits with theoretical expectations for the radio afterglows potentially associated with jets launched in BBH mergers, we find that for jets of energy $\approx 10^{49}$ erg seen on-axis, only jet angles $\theta_{jet} \gtrsim 40^\circ$ are compatible with the observations.

Subject headings: gravitational waves — radiation mechanisms: general — radio continuum: general

1. INTRODUCTION

The recent direct detection of gravitational waves (GWs) from stellar-mass binary black holes (BBHs) by Advanced LIGO (Laser Interferometer Gravitational Wave Observatory) and Virgo has opened a new era in the study of the most exotic objects in the stellar graveyard (Abbott et al. 2016b,a, 2017b,d,c, 2018b). In 2017, the direct detection of GWs from BBHs was awarded the Nobel Prize in Physics. Following that, the remarkable discovery of GW170817 (Abbott et al. 2017e), the first binary neutron star (NS) merger detected in GWs with an electromagnetic (EM) counterpart (Abbott et al. 2017f), helped demonstrate the wide impact of multi-messenger astronomy on a variety of fields, including nucleosynthesis, extreme states of nuclear matter, and cosmology (e.g., Abbott et al. 2017a, 2018a).

According to traditional paradigms, one would not expect to detect EM emission accompanying BBH mergers as the immediate circum-merger environment is expected to be rather clean post merger (i.e., lacking ejecta mass in the merger site). However, the intriguing

ing *Fermi*/GBM 2.9σ -significance detection of a short burst of γ -rays (GRB) possibly associated with the BBH GW150914 (Connaughton et al. 2016, 2018), has spurred the investigation of several new theoretical scenarios for EM emission from BBHs (e.g., Liebling & Palenzuela 2016; Loeb 2016; Perna et al. 2016; Tagawa et al. 2016; Bartos et al. 2017; Dai et al. 2017; de Mink & King 2017; Dolgov & Postnov 2017; Fedrow et al. 2017; Ioka et al. 2017; Kelly et al. 2017; Kimura et al. 2017; Shapiro 2017; D’Orazio & Loeb 2018; Khan et al. 2018). As of today, the question of whether BBH mergers can be accompanied by a release of energy in the form of a relativistic outflow powering a γ -ray counterpart remains open and highly debated (e.g., Bhalerao et al. 2017; Stalder et al. 2017; Verrecchia et al. 2017; Perna et al. 2018, 2019). Certainly, the detection of an EM counterpart to BBHs would start a revolution in the way we have traditionally thought of stellar evolution and accretion processes in astrophysics. Observationally, if at least some BBHs are associated with GRBs, one can hope to strengthen the significance of a potential association by searching for their broad-band afterglows (e.g., Kasliwal et al. 2016; Morsony et al. 2016; Murase et al. 2016; Palliyaguru et al. 2016; Veres et al. 2016; Yamazaki et al. 2016; Perna et al. 2018, 2019). Indeed, the detection of an afterglow from a candidate GRB counterpart to the GW signal would provide a much improved localization (compared to the GW and γ -ray localizations), and constrain key physical parameters such as total kinetic energy of the ejecta, density of the surrounding medium, opening angle of the ejecta, and viewing angle.

Here, we report on a search for a potential radio afterglow from the BBH merger observed by the two LIGO

¹ Department of Physics and Astronomy, Texas Tech University, Box 1051, Lubbock, TX 79409-1051, USA; e-mail: alessandra.corsi@ttu.edu

² Remote Sensing Division, Naval Research Laboratory Washington, DC 20375-5320, USA

³ Department of Physics and Astronomy, Stony Brook University, Stony Brook, NY 11790, USA

⁴ Center for Computational Astrophysics, Flatiron Institute, New York, NY 10010, USA

⁵ Astrophysics Science Division, NASA Goddard Space Flight Center, Mail Code 661, Greenbelt, MD 20771, USA

⁶ Joint Space-Science Institute, University of Maryland, College Park, MD 20742, USA

TABLE 1
X-RAY SOURCES IDENTIFIED BY *Swift*/XRT IN THE ERROR REGION OF GW170608. COLUMNS ARE, FROM LEFT TO RIGHT: SOURCE NUMBER, R.A., DEC., LOCALIZATION ERROR, AND 0.3-10 KEV FLUX. SEE TEXT FOR DISCUSSION.

	R.A. Dec. (hh:mm:ss deg:mm:ss)	Pos. Err. "	F_X ($\text{erg s}^{-1} \text{cm}^{-2}$)
XRT-s1	08:33:03.19+43:12:46.8	8.6	6.1×10^{-13}
XRT-s2	08:32:07.70+43:29:51.0	5.7	1.7×10^{-13}
XRT-s3	08:31:31.70+43:25:48.0	6.3	5.4×10^{-13}
XRT-s4	08:32:52.18+43:23:08.9	6.0	3.7×10^{-13}
XRT-s5	08:34:07.27+43:19:09.1	7.2	4.0×10^{-13}
XRT-s6	08:33:42.79+43:17:21.1	5.0	2.2×10^{-13}
XRT-s7	08:31:12.53+43:25:43.7	7.6	5.1×10^{-13}

detectors on 8 June 2017 UT, henceforth referred to as GW170608 (Abbott et al. 2017c). This is the least massive BBH merger detected by LIGO to date, with component masses of $12_{-2}^{+7} M_{\odot}$ and $7_{-2}^{+2} M_{\odot}$ (90% credible intervals; Abbott et al. 2017c), and a luminosity distance of 340_{-140}^{+140} Mpc (Abbott et al. 2017c).

Several EM observatories around the globe have carried out follow-up observations of at least a portion of the sky localization area of GW170608. Our radio observations with the Karl G. Jansky Very Large Array (VLA), executed under program VLA/16A-206 (PI: Corsi), have targeted the location of a potential high-energy γ -ray transient detected by the *Fermi*/LAT at the 3.5σ significance level, ≈ 1200 s after the GW trigger (Omodei et al. 2017). We supplemented our GHz VLA observations with lower frequency radio observations from the VLA Low-band Ionosphere and Transient Experiment (VLITE).

Here, we present our analysis of the collected VLA and VLITE data, and discuss their implications for models of relativistic ejecta from BBH mergers. Our paper is organized as follows: In Section 2, we summarize the observations that led to the identification of a candidate γ -ray transient in the error area of GW170608. In Section 3, we describe our radio follow-up observations and data reduction. In Section 4, we show how no convincing radio transient was found in association with the *Fermi*/LAT candidate event, and discuss the implications of these results. Finally, in Section 5, we summarize and conclude.

2. GW170608 DETECTION AND CANDIDATE γ -RAY TRANSIENT IDENTIFICATION

The merger associated with the BBH GW170608 was detected by LIGO as a two-detector coincident event at $T_0 = 02:01:16.49$ UT on 2017 June 8. An alert was issued to EM observing partners ≈ 13.5 hrs later, with a sky localization area spanning $\approx 860 \text{ deg}^2$ (90% credible region; Abbott et al. 2017c; The LIGO Scientific Collaboration & Virgo 2017). In response to this alert, several observatories searched their data for potential transients located within the large GW sky area⁷. Among these, the *Fermi*/LAT team performed a search for high-energy transients in data collected during a 10 ks time interval after T_0 (Omodei et al. 2017). The highest significance ($\approx 3.5\sigma$ level) excess found was

found about 1200 s after T_0 at R.A.=08 h 32 m 26.400 s and Dec.=+43 d 23 m 24.00 s (J2000), with a localization uncertainty of 0.24 deg (at 90% confidence). The location of this candidate γ -ray counterpart was occulted by the Earth before $T_0 + 1200$ s. No *Fermi*/GBM counterpart was found for the candidate *Fermi*/LAT transient. The *Fermi*/GBM $3\text{-}\sigma$, 1-second-averaged flux upper limit was in the range $(4.7\text{--}5.6) \times 10^{-7} \text{ erg s}^{-1} \text{ cm}^{-2}$ between about $T_0 + 85$ s and $T_0 + 1$ hr (Goldstein et al. 2017), which at a distance of 340 Mpc corresponds to an isotropic γ -ray energy flux upper-limit of $(6.5\text{--}7.7) \times 10^{48} \text{ erg s}^{-1}$.

The *Swift*/XRT team performed a four-pointing follow up of the possible LAT source, with observations spanning a time interval between ≈ 0.7 d and ≈ 1 d after the GW trigger (Evans et al. 2017). Seven X-ray sources were identified in the observed fields, two of which were previously catalogued (referred to as XRT sources 4 and 5; see Table 1). None of these sources showed evidence for flux variations over *Swift*'s observation period, and none exhibited signs of outburst compared to previous observations. Thus, all of these seven sources were deemed unlikely to being associated with GW170608. For completeness and comparison with our VLA/VLITE results, we report in Table 1 the R.A., Dec. (J2000), localization error, and 0.3-10 keV fluxes of these *Swift*/XRT sources. *Swift*/UVOT observations further revealed that *Swift*/XRT sources 3, 6, and 7 were already present in the SDSS catalog, and none of them exhibited signs of fading over a time interval of $\approx 0.7\text{--}1$ d after the GW trigger (Emery et al. 2017).

Following the identification of the *Fermi*/LAT high-energy candidate transient, several other optical telescopes observed its LAT localization area. The Nanshan One-meter Wide field Telescope (NOWT) team observed the field of the LAT transient in the *R*-band around 15:30:19 UT on 09 June 2017 (Xu et al. 2017). They noted the existence of optical counterparts to *Swift*/XRT sources 1, 3, 6 and 7 in PanSTARRS, DSS-II, and/or SDSS, and excluded evidence for significant optical flux variability of these sources. No optical counterpart was found for source 2 down to $R > 19.2$ mag.

The Arizona Transient Exploration and Characterization (AZTEC) team observed the field of the *Fermi*/LAT candidate in *i* band with the Large Binocular Camera (LBC) mounted on the Large Binocular Telescope (LBT) on beginning on 2017 June 10 (about 2 days post GW trigger; Fong et al. 2017b). The observations covered $\approx 88\%$ of the *Fermi*/LAT localization region, and included the locations of *Swift*/XRT sources 1-4 (see Table 1). No new sources were found in or around the positions of XRT sources 1-4, and no evidence for variability was reported. This same team observed the field of the *Fermi*/LAT candidate also with the Wide Field Camera (WFCAM) on the 3.8-m United Kingdom Infrared Telescope (UKIRT; Fong et al. 2017a), beginning on 2017 Jun 9.2 UT (≈ 1 d after the GW trigger) and 2017 June 10.2 (≈ 2 d after the GW trigger). The first epoch covered the full 90% *Fermi*/LAT localization region, and the positions of the seven *Swift*/XRT sources. The second epoch covered 75% of the *Fermi*/LAT localization area, and the positions of XRT sources 2-7 (see Table 1). Again no new sources or evidence for variability were found (Fong et al. 2017a).

⁷ GRB Coordinates Network Circulars (GCNs) related to the EM follow-up of GW170608 are archived at <https://gcn.gsfc.nasa.gov/other/G288732.gcn3>.

The LIGO error region of GW170608 entered the field of view of the HAWC Cherenkov array about 1 d after T_0 . No evidence for transients at a significance level of $\gtrsim 3\sigma$ was reported in the 0.5-100 TeV band (Smith & Martinez-Castellanos 2017).

The J-GEM collaboration covered almost the entire error region of the *Fermi*/LAT transient candidate, and the location of all *Swift*/XRT sources 1-7, with the 1.05-m Kiso Schmidt telescope. Observations were performed in *i*-band on 2017 June 9.483, 9.489, 9.527, and 9.529 UT, approximately 1.4 d after the GW detection, at a median 5σ depth of $i = 15.6$ mag (AB system). No new transients were found and lack of variability was established for *Swift*/XRT source 7 (Morokuma et al. 2017).

Finally, the Pan-STARRS1 telescope observed the *Fermi*/LAT error circle for 11 nights beginning a day after the GW detection. No new sources were detected within the 90% *Fermi*/LAT localization area of the candidate γ -ray transient at a depth of $i, z \approx 18.5$ mag (within 1 d post merger) and $i, z \approx 20.5$ (daily stacked limits up to 5 d after T_0 , see Smith et al. 2017).

3. RADIO FOLLOW-UP OBSERVATIONS

3.1. VLA observations and data reduction

We observed the field of the *Fermi*/LAT candidate γ -ray counterpart to GW170608 with the VLA at a central frequency of 1.4 GHz, and with a nominal bandwidth of 2 GHz (Corsi 2017). Three observations were carried out on 2017 June 12, June 29, and August 18 UT, all with the VLA in its C configuration. We imaged an area with a nominal ≈ 0.54 deg FWHM primary beam centered around the position of the LAT excess (R.A.=08 h 32 m 30 s, Dec.=+43 d 24 m 00 s), fully enclosing the 90% confidence error area of the LAT localization.

The VLA data were calibrated using the VLA automated pipeline in CASA (McMullin et al. 2007). After calibration, we inspected the data for RFI and applied any necessary flagging. Specifically, data were heavily affected by RFI (which is not uncommon at L-band), reducing the effective bandwidth to $\approx 40\%$ of the nominal ≈ 1 GHz bandwidth of the L-band receiver. Images of the field were formed using the CLEAN algorithm in interactive mode. The FWHM of the major axis of our synthesized beam ranged between $\approx 14''$ – $17''$, consistent with expectations for the VLA in its C configuration. While forming images, we included primary beam corrections to account for the shape of the primary beam up to a region extending to 20% of the power radius, which is the standard option in CLEAN, translating to images of angular diameter ≈ 0.7 deg. Over the three epochs, we reached a typical central image RMS of $\approx 45 \mu\text{Jy}$. The last was estimated with IMSTAT using a circle of radius $60''$ from the center of the images. Our image rms is $\approx 2\times$ higher than expected based on the time spent on-source (≈ 1 h and 20 min), and the actual bandwidth reduction due to RFI. This is due to limited dynamic range of our images related to the presence of bright sources in the crowded field.

After calibration, flagging, and imaging, we visually inspected the images and identified sources with signal-to-noise ratio $\text{SNR} \gtrsim 10$, or flux densities greater than $\approx 450 \mu\text{Jy}$ at 1.4 GHz. At the distance of GW170608 (≈ 340 Mpc), this flux density limit corresponds to a ra-

dio luminosity density of $\approx 6 \times 10^{28} \text{ erg s}^{-1} \text{ Hz}^{-1}$. Our results are reported in Table 3. Source coordinates were calculated with the IMFIT algorithm, using a circular region of radius $10''$ (i.e., of diameter comparable to the FWHM of the synthesized beam), centered around the source position determined through visual inspection. We then used the IMSTAT algorithm to determine the peak flux density of each source within a circular region of radius $10''$ centered around the coordinates obtained via IMFIT. Peak flux errors were calculated by adding in quadrature the RMS noise corrected for primary beam effects (by rescaling the central image RMS by the primary beam correction at the location of each source), and a nominal 5% absolute flux calibration error. Finally, position errors were calculated by dividing the FWHM of the semi-major axis of the synthesized beam by the source signal-to-noise ratio (SNR; peak flux density divided by peak flux density error).

3.2. VLITE observations and data reduction

The VLITE (Clarke et al. 2016) is a commensal, low-frequency system on the VLA that runs in parallel with nearly all observations above 1 GHz. VLITE provides real-time correlation of the signal from a subset of VLA antennas using the low band receiver system (Clarke et al. 2011) and a dedicated DiFX-based software correlator (Deller et al. 2007). The VLITE system processes 64 MHz of bandwidth centered on 352 MHz, but due to strong radio frequency interference (RFI) in the upper portion of the band, the usable frequency range is limited to an RFI-free band of ~ 40 MHz, centered on 338 MHz.

VLITE was operational with 15 working antennas during the VLA 1.4 GHz observations of the *Fermi*/LAT candidate transient on UT 2017 Aug 18. The VLITE data collected during this epoch were processed using a dedicated calibration pipeline, which is based on a combination of the Orbit (Cotton 2008) and AIPS (van Moorsel et al. 1996) data reduction packages. The calibration pipeline uses standard automated tasks for the removal of RFI and follows common techniques of radio-interferometric data reduction, including delay, gain and bandpass calibration (for details on the pipeline data reduction see Polisensky et al. 2016). The flux density scale is set using Perley & Butler (2017) and residual amplitude errors are estimated to be less than 20% (Clarke et al., in preparation). The data were imaged using wide-frequency imaging algorithms in Orbit (task MFimage), by covering the the full primary beam with facets and placing outlier facets on bright sources out to a radius of 20° . Small clean masks are placed on the sources during the imaging process to reduce the effects of CLEAN bias. The pipeline runs two imaging and phase self-calibration cycles before a final image is created.

To improve the quality of the image, the pipeline-calibrated data were re-imaged by hand with MFImage using a higher number of cleaning iterations, which reduced the RMS by a factor of approximately two. The final VLITE image has a restoring beam of $73'' \times 43''$ and a RMS noise of $\approx 2.5 \text{ mJy beam}^{-1}$ (1σ). The image was used to search for counterparts to our VLA sources. These are reported in Table 2 with their position, flux, and errors. Flux densities were measured in AIPS using

a Gaussian fit (JMFIT) and corrected for the primary beam attenuation using factors appropriate for VLITE (Polisensky et al. in preparation). Flux density errors include local image noise and flux scale uncertainty.

4. RESULTS AND DISCUSSION

4.1. Observational results

In our analysis of the 1.4 GHz VLA images of the field of the *Fermi*/LAT candidate γ -ray transient, we have identified a total of 25 radio sources with $SNR \gtrsim 10$, or $F_{1.4\text{GHz}} \gtrsim 450 \mu\text{Jy}$ ($L_{1.4\text{GHz}} \approx 6 \times 10^{28} \text{ erg s}^{-1} \text{ Hz}^{-1}$ at the distance of GW170618). These sources are listed in Table 3. In the most optimistic scenarios for afterglows associated with BBH mergers, $\approx 20\%$ of BBH events occurring in massive (spiral or elliptical) hosts could be associated with GRB-like outflows of radio luminosity density larger than or equal to this value. (see e.g. Figure 8 in Perna et al. 2018).

A comparison of the VLA sources (Table 3) with those found by the *Swift*/XRT team in the GW error region (Table 1) shows that only two of the *Swift*/XRT sources are within a distance of $2'$ from any of our VLA sources. Specifically, *Swift*/XRT-s1 and *Swift*/XRT-s2 are located within $\approx 0.9'$ of our VLA source S13 and S20, respectively. We note that at the distance of GW170608 ($\approx 340 \text{ Mpc}$), an angular radius of $2'$ corresponds to a physical distance of about 170 kpc. As shown by Perna et al. (2018), this radial distance is likely to enclose the host galaxy of $\gtrsim 70 - 90\%$ of BBH mergers occurring in massive hosts (see their Figure 3). Thus, searching for sources located within $2'$ of the position of our VLA sources leaves room to find not only coincident counterparts but also potential host galaxies.

We also searched for any counterpart to our VLA sources in VLITE images. Only a few of the VLA sources were found with $SNR \gtrsim 5$ (or flux density $\gtrsim 12.5 \text{ mJy}$) in the VLITE image taken on 2017 August 18 UT at 338 MHz. These V1-7 sources are reported in Table 2. They were unresolved at the angular resolution of the image ($73'' \times 43''$).

To gain additional information on the possible nature of the 25 sources identified in our VLA images, we searched for previously known sources co-located with them. To this end, we queried the catalogs by the National VLA Sky Survey (NVSS), the VLA FIRST, and the NASA/IPAC Extra-galactic Database (NED). Table 3 reports information about the closest (in terms of sky position, considering position errors) and most similar (in terms of radio flux) previously known radio source found within $2'$ of each of our VLA sources. When a previously known radio source is indeed found, we classify it as RadioS in Table 3, and report its R.A. and Dec., radio peak flux density, and position uncertainty. The position uncertainty corresponds to the semi-major position uncertainty as reported in NED for all sources with an NVSS counterpart (Condon et al. 1998). For FIRST sources, we divide the FWHM of the semi-major axis of the synthesized beam by the source signal-to-noise ratio, where the last takes into account the clean bias of 0.25 mJy which is added to all peak fluxes reported in FIRST⁸. Because of systematic uncertainties, any posi-

tion error smaller than $0.1''$ in Table 3 is set equal to this systematic uncertainty value. If a radio source is not found within $2'$, we report in the Table 3 only information about the classification of the closest known source found in NED (see sources S17-S20 and S24-25 in Table 3).

Overall, all of the 25 radio sources we found in our VLA images are associated with previously known sources located within $2'$. All but six of the VLA sources have an NVSS or FIRST counterpart within $2'$. The known sources found in association with our VLA sources S4, S19, and S24-S25 show offsets larger than the estimated position errors, so they could be either unrelated sources (as most likely for S25), or potential host galaxies. Incidentally we note that the radio source coincident with S22 is a galaxy located at a distance much farther than that of GW170608. No NVSS/FIRST sources are found in coincidence with our VLA S17-S20 and S24-25, and this is not surprising considering that the VLA 1.4 GHz peak flux densities of these sources are close or below the FIRST/NVSS catalog completeness limits of $\approx 0.75 \text{ mJy} / 2.5 \text{ mJy}$ (White et al. 1997; Condon et al. 1998).

None of the 25 sources identified in our VLA images showed any evidence for significant variability within the timescales of our 3 VLA epochs, which covered days 4, 21, and 67 since the BBH merger. Although large uncertainties affect predictions for radio emission from BBHs, the lack of variability on these timescales strongly suggests that all of the identified VLA sources are unrelated to possible afterglow-like emission from the *Fermi*/LAT candidate. Specifically, in the standard synchrotron model for radio emission from fast GRB ejecta, one would expect a post-peak temporal evolution of the optically thin radio afterglow such that $F_{1.4\text{GHz}} \propto (t/t_{\text{peak}})^{-0.75} - (t/t_{\text{peak}})^{-1.1}$ (Perna et al. 2018, and references therein), which would ensure flux variations of a factor of $\gtrsim 2$ between successive epochs of our follow-up campaign.

4.2. Constraints on the presence of a relativistic jet

Given the lack of a radio counterpart to the candidate *Fermi*/LAT transient, our VLA observations constrain the flux density of any potential radio afterglow to $F_{1.4\text{GHz}} \lesssim 450 \mu\text{Jy}$. We thus explore whether this constraint can rule out at least some portions of the parameter space allowed for a relativistic jet potentially produced in association with the GW170608 merger. Light curves for jets propagating in the clean environment expected around BBH mergers (i.e. one that lacks ejecta mass in the merger site) have been computed by Perna et al. (2019). We use their online library⁹ to derive the model radio luminosities at 1.4 GHz, and compare them with our limits. The models are characterized by the jet energy E_{jet} and the angle θ_{jet} over which the bulk of the energy is distributed. For any of these parameters, the luminosity is then a strong function of the viewing angle with the jet axis, and the time of the observation. We set the last to 4 d after the merger for comparison with our VLA observations, as this is the most constraining epoch. For the viewing angle, we assume that our line of sight is along the jet axis (given the potential detection of a *Fermi*/LAT high-energy transient and the GW selection

⁸ See <http://sundog.stsci.edu/first/catalogs/readme.html> for information about the FIRST survey.

⁹ <http://www.astro.sunysb.edu/rosalba/EMmod/models.html>

TABLE 2

VLITE COUNTERPARTS TO VLA SOURCES. COLUMNS ARE, FROM LEFT TO RIGHT: SOURCE NUMBER, VLA COINCIDENT SOURCE NUMBER, R.A., DEC., POSITION ERROR, AND FLUX DENSITY AS MEASURED IN THE VLITE IMAGE. S4/S6 AND S10/S11 ARE DETECTED AS ONE SINGLE SOURCE BY VLITE.

VLA #		R.A. Dec.	Pos. Err.	$F_{338\text{ MHz}}$
		(hh:mm:ss deg:mm:ss)	(")	(mJy)
V1	S1	08:33:16.53 +43:23:50.1	9.43	15.1 ± 3.9
V2	S2	08:31:25.95 +43:25:13.4	7.30	523.9 ± 104.8
V3	S3	08:32:43.15 +43:14:38.1	7.37	100.1 ± 20.2
V4	S4 + S6	08:32:28.64 +43:02:56.1	7.30	380.8 ± 76.2
V5	S5	08:31:11.47 +43:16:08.7	7.85	32.1 ± 6.9
V6	S7	08:31:00.19 +43:27:27.9	8.07	26.7 ± 5.9
V7	S10 + S11	08:33:49.38 +43:20:25.0	7.35	127.2 ± 25.6

effects which favor a face-on orientation for detection). This “down-the-barrel” assumption for the line-of-sight is the most constraining one. In fact, viewing angles with $\theta_{\text{obs}} > \theta_{\text{jet}}$ would lead to weaker constraints on the energetics than the ones we present in what follows (in other words, higher jet energies would be allowed for larger viewing angles).

Figure 1 shows a comparison of the on-axis jet luminosity for a range of relativistic jets (Lorentz factor of $\Gamma = 100^{10}$) with energies varying between $10^{46} - 10^{49}$ ergs, and opening angles between $10^\circ - 40^\circ$. These models were chosen to bracket the energetics of the candidate *Fermi* counterpart to GW150914 (Connaughton et al. 2016, 2018) which had an isotropic inferred energy of $\approx 10^{49}$ ergs, which translates into a jet energy of $10^{49}(1 - \cos\theta_{\text{jet}})$ ergs. The dashed lines in Fig. 1 mark the range of observational upper limits on the radio luminosity density corresponding to the uncertainty on the distance in GW170608 (i.e. $L_{1.4\text{ GHz}} \approx (2.1 - 12) \times 10^{28} \text{ erg s}^{-1} \text{ Hz}^{-1}$). As evident from this Figure, for a jet of energy $E_{\text{jet}} = 10^{49}$ ergs, only jet angles $\theta_{\text{jet}} \gtrsim 40^\circ$ are compatible with the full range for the flux limit. It is interesting to discuss this limit in light of the constraints derived by Perna et al. (2018) for GW150914. The fact that GW150914 was the only γ -ray candidate out of 10 BBH detections in the O1/O2 observing runs led to the limit $(E_{\text{iso}}/10^{49}\text{erg})(\theta_{\text{jet}}/20^\circ) \lesssim 1$. In the case of GW170608, the constraint $\theta_{\text{jet}} \gtrsim 40^\circ$ with $E_{\text{jet}} = 10^{49}$ ergs is equivalent to $E_{\text{iso}} \lesssim 4.2 \times 10^{49}$ erg, which is still compatible with the statistical constraint previously derived from GW150914.

We should finally note that the afterglow models here presented are computed for a typical interstellar density of $n = 0.01 \text{ cm}^{-3}$ (Perna et al. 2018). However, the flux brightness scales roughly as $n^{1/2}$ for a range of conditions (Sari et al. 1998). Hence, merger events in lower densities could be more energetic and still be below the observational limits, while mergers in denser regions would be constrained to being less energetic.

5. SUMMARY AND CONCLUSION

We have presented radio follow-up observations of a *Fermi*/LAT candidate transient identified in the error region of GW170608, a BBH merger discovered by the LIGO detectors. Our observations with the VLA

¹⁰ For the same model parameters, lower Lorentz factors yield lower luminosities. E.g, for $\Gamma = 10$ the brightest point in Fig. 1 would be 80% of the one for $\Gamma = 100$.

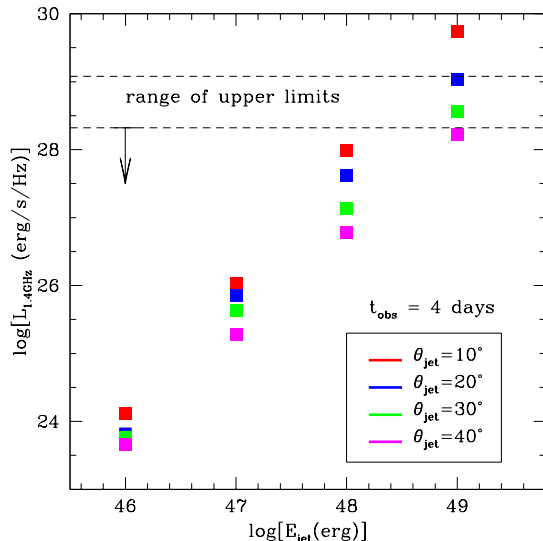


FIG. 1.— 1.4 GHz luminosity density at 4 d after the merger, from a relativistic jet with Lorentz factor $\Gamma = 100$ seen on axis. Models are considered for a range of jet energies E_{jet} and opening angles θ_{jet} of the jet. The dashed lines mark the region of upper limits on the 1.4 GHz luminosity density derived from our VLA observations given the uncertainties on the estimated distance of GW170608. See text for discussion.

at 1.4 GHz were complemented with VLITE data at 338 MHz. We identify 25 sources with $SNR \gtrsim 10$ in the crowded VLA images of the LAT field. A few of these also had a counterpart with $SNR \gtrsim 5$ in VLITE data. Over the three epochs of our VLA follow up, none of the sources showed evidence for significant variability. Based on the lack of variability, we conclude that it is very unlikely that any of the VLA sources in our field are associated with the radio afterglow of the *Fermi*/LAT candidate burst.

We have compared the limits derived from our VLA observations with theoretical expectations for the radio afterglows potentially associated with jets launched in BBH mergers (Perna et al. 2019). Altogether, our analysis shows the key role that broad-band follow ups to GW events can play to gradually restrict the allowed parameter space for electromagnetically bright, relativistic outflows driven by the merger of two BHs.

With this study we have demonstrated the feasibility of radio follow-up observations that, in the near-future

observing runs of the advanced LIGO and Virgo detectors, could clarify the fundamental physics question of whether BBH mergers can be accompanied by relativistic outflows powering GRB-like bursts and afterglows. With the number of well-localized BBH mergers destined to increase thanks to the improving sensitivity of ground-based GW detectors, and with the Virgo interferometer joining the two LIGO detectors for longer observing runs (Abbott et al. 2016), it is crucial that the community maintains active follow-up efforts of nearby BBHs. If appropriately planned, these follow-up efforts may ultimately help us identify a BBH afterglow, or set constraining upper-limits on the numerous models that have been proposed in the literature to explain the still largely debated, possible association between GW150914 and a *Fermi*/GBM γ -ray transient.

We finally note that commensal VLITE observation

could also uncover potential coherent radio emission generated near the instant of merger. The last, in turn, could probe the immediate magnetic environment and the properties of the intergalactic medium (Callister et al. 2019).

K.A., R.S., and A.C. acknowledge support from the NSF CAREER award #1455090. R.P. acknowledges support from the NSF under grant AST-1616157. Basic research in radio astronomy at the Naval Research Laboratory is supported by 6.1 Base funding. The Center for Computational Astrophysics at the Flatiron Institute is supported by the Simons Foundation. The National Radio Astronomy Observatory is a facility of the National Science Foundation operated under cooperative agreement by Associated Universities, Inc. We thank Dale Frail, Mansi Kasliwal, Namir Kassim, and Nipuni Palliyaguru for constructive comments.

REFERENCES

- Abbott, B. P., Abbott, R., Abbott, T. D., et al. 2016a, *Physical Review Letters*, 116, 241103
- . 2016b, *Physical Review Letters*, 116, 061102
- Abbott, B. P., et al. 2016, *Living Reviews in Relativity*, 19, 1
- Abbott, B. P., Abbott, R., Abbott, T. D., et al. 2017a, *Nature*, 551, 85
- . 2017b, *Physical Review Letters*, 118, 221101
- . 2017c, *ApJ*, 851, L35
- . 2017d, *Physical Review Letters*, 119, 141101
- . 2017e, *Physical Review Letters*, 119, 161101
- . 2017f, *ApJ*, 848, L12
- . 2018a, *Physical Review Letters*, 121, 161101
- . 2018b, arXiv e-prints, arXiv:1811.12907
- Bartos, I., Kocsis, B., Haiman, Z., & Márka, S. 2017, *ApJ*, 835, 165
- Bhalerao, V., Kasliwal, M. M., Bhattacharya, D., et al. 2017, *ApJ*, 845, 152
- Callister, T. A., Anderson, M. M., Hallinan, G., et al. 2019, arXiv e-prints, arXiv:1903.06786
- Clarke, T. E., Kassim, N. E., Briskin, W., et al. 2016, in *Proc. SPIE*, Vol. 9906, *Ground-based and Airborne Telescopes VI*, 99065B
- Clarke, T. E., Perley, R. A., Kassim, N. E., et al. 2011, in *General Assembly and Scientific Symposium, 2011 XXXth URSI*
- Condon, J. J., Cotton, W. D., Greisen, E. W., et al. 1998, *AJ*, 115, 1693
- Connaughton, V., Burns, E., Goldstein, A., et al. 2016, *ApJ*, 826, L6
- . 2018, *ApJ*, 853, L9
- Corsi, A. 2017, *GRB Coordinates Network*, 21253
- Cotton, W. D. 2008, *PASP*, 120, 439
- Dai, L., McKinney, J. C., & Miller, M. C. 2017, *MNRAS*, 470, L92
- de Mink, S. E., & King, A. 2017, *ApJ*, 839, L7
- Deller, A. T., Tingay, S. J., Bailes, M., & West, C. 2007, *PASP*, 119, 318
- Dolgov, A., & Postnov, K. 2017, *Jcap*, 9, 018
- D’Orazio, D. J., & Loeb, A. 2018, *Phys. Rev. D*, 97, 083008
- Emery, S. W. K., Oates, S. R., Barthelmy, S. D., et al. 2017, *GRB Coordinates Network*, 21235
- Evans, P. A., Kennea, J. A., Barthelmy, S. D., et al. 2017, *GRB Coordinates Network*, 21233
- Fedrow, J. M., Ott, C. D., Spherhake, U., et al. 2017, *Physical Review Letters*, 119, 171103
- Fong, W., Milne, P., Smith, N., Zaritsky, D., et al. 2017a, *GRB Coordinates Network*, 21245
- Fong, W., Rothberg, B., Hill, J., et al. 2017b, *GRB Coordinates Network*, 21244
- Goldstein, A., Hamburg, R., Wilson-Hodge, C., & et al. 2017, *GRB Coordinates Network*, 21263
- Ioka, K., Matsumoto, T., Teraki, Y., Kashiyama, K., & Murase, K. 2017, *MNRAS*, 470, 3332
- Kasliwal, M. M., Cenko, S. B., Singer, L. P., et al. 2016, *ApJ*, 824, L24
- Kelly, B. J., Baker, J. G., Etienne, Z. B., Giacomazzo, B., & Schnittman, J. 2017, *Phys. Rev. D*, 96, 123003
- Khan, A., Paschalidis, V., Ruiz, M., & Shapiro, S. L. 2018, *Phys. Rev. D*, 97, 044036
- Kimura, S. S., Takahashi, S. Z., & Toma, K. 2017, *MNRAS*, 465, 4406
- Liebling, S. L., & Palenzuela, C. 2016, *Phys. Rev. D*, 94, 064046
- Loeb, A. 2016, *ApJ*, 819, L21
- McMullin, J. P., Waters, B., Schiebel, D., Young, W., & Golap, K. 2007, in , *Astronomical Data Analysis Software and Systems XVI (ASP Conf. Ser. 376)*
- Morokuma, T., Tanaka, M., Tominaga, N., et al. 2017, *GRB Coordinates Network*, 21249
- Morsony, B. J., Workman, J. C., & Ryan, D. M. 2016, *ApJ*, 825, L24
- Murase, K., Kashiyama, K., Mészáros, P., Shoemaker, I., & Senno, N. 2016, *ApJ*, 822, L9
- Omodei, N., Kocevski, D., Vianello, G., et al. 2017, *GRB Coordinates Network*, 21227
- Palliyaguru, N. T., Corsi, A., Kasliwal, M. M., et al. 2016, *ApJ*, 829, L28
- Perna, R., Chruslinska, M., Corsi, A., & Belczynski, K. 2018, *MNRAS*, 477, 4228
- Perna, R., Lazzati, D., & Farr, W. 2019, arXiv e-prints, 1901.04522, arXiv:1901.04522
- Perna, R., Lazzati, D., & Giacomazzo, B. 2016, *ApJ*, 821, L18
- Polisensky, E., Lane, W. M., Hyman, S. D., et al. 2016, *ApJ*, 832, 60
- Sari, R., Piran, T., & Narayan, R. 1998, *ApJ*, 497, L17
- Shapiro, S. L. 2017, *Phys. Rev. D*, 95, 101303
- Smith, A. J., & Martinez-Castellanos, I. 2017, *GRB Coordinates Network*, 21248
- Smith, K. W., Chambers, K. C., Huber, M. E., et al. 2017, *GRB Coordinates Network*, 21262
- Stalder, B., Tonry, J., Smartt, S. J., et al. 2017, *ApJ*, 850, 149
- Tagawa, H., Umemura, M., & Gouda, N. 2016, *MNRAS*, 462, 3812
- The LIGO Scientific Collaboration, & Virgo. 2017, *GRB Coordinates Network*, 21221
- van Moorsel, G., Kemball, A., & Greisen, E. 1996, in , *Astronomical Data Analysis Software and Systems V*, 37
- Veres, P., Preece, R. D., Goldstein, A., et al. 2016, *ApJ*, 827, L34
- Verrecchia, F., Tavani, M., Ursi, A., et al. 2017, *ApJ*, 847, L20
- White, R. L., Becker, R. H., Helfand, D. J., & Gregg, M. D. 1997, *ApJ*, 475, 479
- Xu, D., Liu, J. Z., Niu, H. B., et al. 2017, *GRB Coordinates Network*, 21236
- Yamazaki, R., Asano, K., & Ohira, Y. 2016, *Progress of Theoretical and Experimental Physics*, 2016, 051E01

TABLE 3

RESULTS OF THE THREE EPOCHS OF OUR VLA FOLLOW-UP CAMPAIGN OF GW170608 AT 1.4 GHz. COLUMNS ARE, FROM LEFT TO RIGHT: SOURCE NAME; R.A. AND DEC. FROM OUR VLA IMAGES; OBJECT CLASS (RadioS FOR ALL SOURCES WITH A COUNTERPART WITHIN $2''$ OF THE VLA POSITION IN FIRST (F) OR NVSS (N), OR OBJECT CLASS OF THE CLOSEST SOURCE WITHIN $2''$ FOUND IN NED IF NO NVSS/FIRST COUNTERPART IS PRESENT); MODIFIED JULIAN DATE (MJD) OF OUR VLA OBSERVATIONS; EPOCH IN DAYS SINCE GW170608 DISCOVERY; VLA FLUX DENSITY; NVSS OR FIRST FLUX DENSITY (WHEN AVAILABLE); OFFSET BETWEEN THE SOURCE LOCATION AS MEASURED IN OUR VLA IMAGES AND THAT REPORTED IN NVSS OR FIRST, OR (IF NOT AVAILABLE) OFFSET OF THE CLOSEST SOURCE REPORTED IN NED; VLA POSITION ERROR; NVSS OR FIRST POSITION ERROR.

Name	R.A. Dec. (VLA)	Class	Epoch	ΔT	$F_{1.4\text{ GHz}}$ (VLA)	$F_{1.4\text{ GHz}}$ (NVSS/ FIRST)	Offset	Pos.Err. (VLA)	Pos.Err. (NVSS/ FIRST)
	(hh:mm:ss deg:mm:ss)		(MJD)	(day)	(mJy)	(mJy)	($''$)	($''$)	($''$)
S1	08:33:16.15+43:23:51.01	RadioS(F)	57917.333	4	3.12 ± 0.40	3.66 ± 0.22	0.30	0.35	0.11
	" "	"	57933.500	21	3.16 ± 0.17	"	"	0.44	"
	" "	"	57983.500	67	2.86 ± 0.16	"	"	0.47	"
S2	08:31:26.13+43:25:12.49	RadioS(N)	57917.333	4	98.4 ± 4.9	149 ± 4.5	0.52	0.34	1.50
	" "	"	57933.500	21	110.0 ± 5.5	"	"	0.41	"
	" "	"	57983.500	67	109.1 ± 5.5	"	"	0.43	"
S3	08:32:43.30+43:14:36.05	RadioS(N)	57917.333	4	31.5 ± 1.6	43.0 ± 1.4	0.94	0.34	0.5
	" "	"	57933.500	21	33.4 ± 1.7	"	"	0.41	"
	" "	"	57983.500	67	31.7 ± 1.6	"	"	0.43	"
S4	08:32:29.39+43:02:58.04	RadioS(N)	57917.333	4	24.7 ± 1.3	196.6 ± 4.6	6.3	0.35	1.5
	" "	"	57933.500	21	26.6 ± 1.4	"	"	0.42	"
	" "	"	57983.500	67	29.5 ± 1.5	"	"	0.44	"
S5	08:31:11.34+43:16:06.66	RadioS(F)	57917.333	4	11.6 ± 0.1	10.4 ± 0.54	0.60	0.72	0.1
	" "	"	57933.500	21	13.4 ± 0.7	"	"	0.42	"
	" "	"	57983.500	67	12.8 ± 0.7	"	"	0.44	"
S6	08:32:28.84+43:03:20.21	RadioS(F)	57917.333	4	17.99 ± 0.93	22.5 ± 1.1	1.5	0.35	0.1
	" "	"	57933.500	21	22.83 ± 1.16	"	"	0.42	"
	" "	"	57983.500	67	18.29 ± 0.95	"	"	0.45	"
S7	08:31:00.04+43:27:28.96	RadioS(F)	57917.333	4	9.22 ± 0.16	12.61 ± 0.65	1.3	0.53	0.1
	" "	"	57933.500	21	8.96 ± 0.45	"	"	0.42	"
	" "	"	57983.500	67	8.82 ± 0.46	"	"	0.45	"
S8	08:31:14.21+43:11:19.64	RadioS(F)	57917.333	4	2.11 ± 0.16	2.45 ± 0.18	0.7	0.95	0.16
	" "	"	57933.500	21	2.76 ± 0.17	"	"	0.70	"
	" "	"	57983.500	67	2.32 ± 0.18	"	"	0.79	"
S9	08:32:56.03+43:13:24.65	RadioS(F)	57917.333	4	5.43 ± 0.47	6.19 ± 0.34	0.6	0.35	0.1
	" "	"	57933.500	21	4.60 ± 0.24	"	"	0.43	"
	" "	"	57983.500	67	4.95 ± 0.26	"	"	0.45	"
S10	08:33:50.53+43:20:39.09	RadioS(F)	57917.333	4	7.82 ± 0.29	3.55 ± 0.23	1.3	0.37	0.29
	" "	"	57933.500	21	7.52 ± 0.39	"	"	0.43	"
	" "	"	57983.500	67	7.16 ± 0.37	"	"	0.45	"
S11	08:33:48.59+43:20:04.31	RadioS(F)	57917.333	4	5.14 ± 0.19	2.15 ± 0.18	1.0	0.42	0.57
	" "	"	57933.500	21	4.50 ± 0.25	"	"	0.46	"
	" "	"	57983.500	67	4.86 ± 0.27	"	"	0.48	"
S12	08:31:20.18+43:33:00.13	RadioS(F)	57917.333	4	3.62 ± 0.28	3.9 ± 0.2	1.4	0.37	0.11
	" "	"	57933.500	21	3.61 ± 0.20	"	"	0.47	"
	" "	"	57983.500	67	4.13 ± 0.23	"	"	0.49	"
S13	08:33:05.09+43:13:37.07	RadioS(F)	57917.333	4	2.14 ± 0.13	2.44 ± 0.18	0.60	0.42	0.19
	" "	"	57933.500	21	2.26 ± 0.13	"	"	0.48	"
	" "	"	57983.500	67	1.99 ± 0.13	"	"	0.55	"
S14	08:32:45.34+43:29:49.34	RadioS(F)	57917.333	4	1.59 ± 0.19	1.81 ± 0.16	0.40	0.36	0.20
	" "	"	57933.500	21	1.48 ± 0.09	"	"	0.50	"
	" "	"	57983.500	67	1.31 ± 0.09	"	"	0.57	"
S15	08:32:08.63+43:40:05.18	RadioS(N)	57917.333	4	3.65 ± 0.15	3.8 ± 0.5	3.1	0.66	9.1
	" "	"	57933.500	21	3.30 ± 0.21	"	"	0.52	"
	" "	"	57983.500	67	3.20 ± 0.21	"	"	0.58	"
S16	08:32:59.90+43:40:03.57	RadioS(N)	57917.333	4	3.90 ± 0.23	4.00 ± 0.5	0.88	0.44	11
	" "	"	57933.500	21	3.05 ± 0.20	"	"	0.55	"
	" "	"	57983.500	67	3.51 ± 0.23	"	"	0.57	"
S17	08:31:53.81+43:27:20.12	Galaxy	57917.333	4	0.99 ± 0.20	-	1.6	0.36	-
	" "	"	57933.500	21	1.05 ± 0.07	-	"	0.57	-
	" "	"	57983.500	67	0.65 ± 0.07	-	"	0.86	-
S18	08:32:24.99+43:18:26.14	Galaxy	57917.333	4	0.67 ± 0.06	-	0.72	0.52	-
	" "	"	57933.500	21	0.88 ± 0.06	-	"	0.59	-
	" "	"	57983.500	67	0.64 ± 0.06	-	"	0.83	-
S19	08:33:04.28+43:32:37.78	UvS	57917.333	4	1.12 ± 0.09	-	7.7	0.60	-
	" "	"	57933.500	21	0.98 ± 0.08	-	"	0.70	-
	" "	"	57983.500	67	0.99 ± 0.09	-	"	0.78	-
S20	08:32:02.84+43:29:45.43	Galaxy	57917.333	4	0.89 ± 0.07	-	1.1	0.55	-
	" "	"	57933.500	21	0.75 ± 0.06	-	"	0.70	-
	" "	"	57983.500	67	0.85 ± 0.07	-	"	0.74	-

Name	R.A. Dec. (VLA)	Class	Epoch	ΔT	$F_{1.4\text{ GHz}}$ (VLA)	$F_{1.4\text{ GHz}}$ (NVSS/ FIRST)	Offset	Pos.Err. (VLA)	Pos.Err. (NVSS/ FIRST)
	(hh:mm:ss deg:mm:ss)		(MJD)	(day)	(mJy)	(mJy)	($''$)	($''$)	($''$)
S21	08:32:12.72 +43:23:06.47	RadioS(F)	57917.333	4	1.61 ± 0.10	1.29 ± 0.15	0.70	0.39	0.65
	" "		57933.500	21	1.72 ± 0.10	"	"	0.46	"
	" "		57983.500	67	1.70 ± 0.10	"	"	0.50	"
S22	08:32:05.46 +43:17:27.99	RadioS(F)	57917.333	4	1.69 ± 0.09	2.01 ± 0.17	0.50	0.42	0.26
	" "		57933.500	21	1.84 ± 0.10	"	"	0.47	"
	" "		57983.500	67	1.76 ± 0.10	"	"	0.51	"
S23	08:32:19.72 +43:16:11.42	RadioS(F)	57917.333	4	1.49 ± 0.07	1.73 ± 0.16	0.60	0.56	0.28
	" "		57933.500	21	1.54 ± 0.09	"	"	0.49	"
	" "		57983.500	67	1.44 ± 0.09	"	"	0.55	"
S24	08:32:43.90 +43:10:43.91	Galaxy	57917.333	4	0.85 ± 0.11	-	14	0.49	-
	" "		57933.500	21	0.92 ± 0.09	-	"	0.79	-
	" "		57983.500	67	0.88 ± 0.10	-	"	0.94	-
S25	08:32:35.05 +43:33:46.81	Star	57917.333	4	0.87 ± 0.08	-	7.4	0.62	-
	" "		57933.500	21	0.67 ± 0.07	-	"	0.87	-
	" "		57983.500	67	0.78 ± 0.08	-	"	0.89	-